ASSESSMENT OF MULTALL AS CFD CODE FOR THE ANALYSIS OF TUBE-AXIAL FANS

Piero Danieli[1], Massimo Masi[2] *, Giovanni Delibra[3], Alessandro Corsini[3], Andrea Lazzaretto[1]

[1]University of Padova, Department of Industrial Engineering, Padova, Italy
[2]University of Padova, Department of Management and Engineering, Vicenza, Italy
[3]"«Sapienza» University of Roma, Department of Aerospace Engineering, Roma, Italy

*corresponding author's email: massimo.masi@unipd.it

ABSTRACT

This work deals with the application of the open source CFD code MULTALL to the analysis of tube-axial-fans. The code has been widely validated in the literature for high-speed turbomachine flows but not applied yet to low speed tutbomachines. The aim of this work is to assess the degree of reliability of MULTALL as a tool for simulating the internal flow in industrial axial-flow fan rotors. To this end, the predictions of the steady-state air flow field in the annular sector of a 315mm tube-axial fan obtained by MULTALL 18.3 are compared with those obtained by two state-of-the-art CFD codes and experimental data of the global aerodynamic performance of the fan and the pitch-wise averaged velocity distribution downstream of the rotor. All the steady-state RANS calculations were performed on either fully structured hexahedron or hexa-dominant grids using classical formulations of algebraic turbulence models. The pressure curve and the trend of the aeraulic efficiency in the stable operation range of the fan predicted by MULTALL show very good agreement with both the experimental data and the other CFD results. Although the estimation of the fan efficiency predicted by MULTALL can be noticeably improved by the more sophisticated state-of-the-art CFD codes, the analysis of the velocity distribution at the rotor exit supports the use of MULTALL as a reliable CFD analysis tool for designers of low-speed axial fans.

Keywords: Axial-flow fans, MULTALL, CFD of low hub-to-tip ratio axial fans, Experimental velocity profiles, 5-hole 3D probe.

INTRODUCTION

The design of a high-efficiency industrial fan requires the consideration of a wide set of geometric parameters [1]. The number of these parameters may be still incompatible with the time needed to build-up and run high fidelity state-of-the-art RANS computations (for example, up to 26 parameters have been considered in [1]). In this context, it is interesting to investigate the capabilities of past generation CFD codes, originally conceived for a scenario of very limited availability of computational power, because they could allow very fast analyses with present-day computers. The objective of this work is the application of the open source CFD code MULTALL 18.3 to the analysis of tube-axial-fans. MULTALL belongs to the so-called `density-based´ CFD codes, which link momentum and continuity equations by means of the mass density of the fluid. Theory and applications of these computational methods can be found in [2]. MULTALL was originally developed for the two-dimensional modelling of the internal flow in multistage axial-flow steam and gas turbines [3]. Further improvements first dealt with the implementation of non-overlapping grids and with the use of the multi-grid technique to accelerate convergence [4]. Thanks to the improvements in computing resources, fully 3-dimensional (3D) simulations have become the new standard [5, 6] and the code was updated to include the mixing plane approach in order to manage the interfaces between blade rows in multistage turbines [7]. Most of the methods and techniques implemented in the year 2000 release of the code are well summarised in [8] and were validated during the next few years with an increasing number of specific axial-flow turbine applications ranging from tip leakage flow analyses [9, 10] to unsteady operation [11]. More recently, the applicability of the code has been extended to compressors, high-speed fans and mixed-to-radial inflow turbomachines [12-14]. Finally, in 2017, the author, prof. John Denton, made MULTALL available as an open source code [15].

The complexity and strong unsteadiness of the internal flow in many types of turbomachines has driven the development of CFD codes. State-of-the-art codes are able to analyse turbomachines flow using several methods based on either unsteady RANS calculation on moving grids or steady-state calculations with the Multi-Reference-Frame (MFR) approach and several sliding interface models, including very advanced turbulence treatments [16]. In contrast, in many instances the internal flow of the tube-axial fan can be simulated by RANS-CFD with a rather high accuracy by relative-flow calculations of single-blade passage, at least when dealing with the aerodynamic performance within the stable operation range [17, 18]. Accordingly, the modelling options provided in MULTALL appear suited to simulate quite easily the steady-state operation of axial industrial fans. However, there are no references in the scientific literature showing the capabilities of MULTALL to simulate the internal flow in such types of low-speed turbomachines. The aim of this paper is twofold: (i) assessing the suitability of MULTALL to perform tube-axial fan simulations by comparing its predictions with those obtained by two state-of-the-art CFD codes and (ii) proposing an approach for the analysis of the flow field in tube-axial fans based on MULTALL and validating the results with experimental data. To this end, the paper: describes the main design features of the 315mm tube-

axial fan used as a benchmark for the CFD simulations; presents the experimental and numerical methods and compares CFD results and experimental data. The compared parameters are the fan pressure and efficiency curves, measured according to the ISO 5801 standard [19], and local velocity measurements downstream of the rotor, obtained by a five-hole probe.

1 The USW28 fan

The USW28 tube-axial fan is a prototype of an industrial machine designed in accordance with the design method suggested in [20]. The dimensionless performance coefficients at the design point are $\Phi_D = 0.097$ and $\Psi_D = 0.017$. According to the preliminary design, the arbitrary vortex blading should assure a constant swirl at the rotor exit with a tangential velocity ratio $\varepsilon_S = 0.48$ when the blade positioning angle ϕ_P is equal to 20°. Figure 1 shows two pictures of the USW28 fan rotor, and Tab. 1 reports all the main specifications of the fan geometry. All the details of the USW28 design are deeply discussed in [20].

TABLE 1: DETAILS OF THE USW28 FAN

Global features of the fan						
D [mm]	ν [--]	Z [--]	AR [--]	ξ_t [°]	tc/l [%]	R_a span/chord** [μm]
315	0.28	10	3.04	69.3	2.7	18.6/11.4

Aerofoil's features **F-Series: circular arc meanline with C4 thickness distribution** ‡					
camber		**maximum thickness**	**nose droop**	**lift coefficient**	**incidence angle**
h/l [%]	θ [°]	t/l [%]	d/l [-]	C_L§ [-]	i [°]
4.4	19.91	10	0.02	0.8	-3.81

** *measured along the blade span/chord direction*
‡ Wallis, R., A., 1977, "The F-Series airfoils for fan blade sections", Mech. Eng. Trans. I. E. Aust., ME2 Vol. 1, pp.12-20
§ *at 3.46° attack angle of the section without nose droop*

Blade sections features						
section ID	**radial position** x [-]	**chord** chord/l [-]	**solidity** σ [-]	**loading factor** σC_L [°]	**stagger** ξ [°]	**position** ϕ_P [°]
1 (hub)	0.281	0.96	1.27	1.019	36	51.5
2	0.380	1	0.93	0.740	47.3	40.2
3	0.518	1	0.71	0.571	54.7	32.9
4 (MS)	0.637	1	0.58	0.465	59.7	28.1
5	0.815	1	0.45	0.363	64.8	23.3
6 (tip)	0.993	1	0.37	0.298	68.2	20.1

FIGURE 1: FRONT (LEFT) AND REAR (RIGHT) VIEWS OF THE USW28 FAN ROTOR.

2 Instruments and Method

Table 2 lists the tools subject of this section and summarises the methods used to verify their suitability to the aim of the work.

TABLE 2: TOOLS AND METHODS

Available tools				
Tools	CFD		EFD	
	MULTALL-	- CCM+ - OpenFoam	ISO 5801 test rig	Five-hole 3D probe
Assessment of the tools				
Method	Sensitivity study on: - Grid density - Domain size - Turbulence model		Comparison between previous [20] and new measurements	Comparison between data and theoretical velocity profiles

2.1 Experimental Fluid Dynamics

The layout of the full experimental setup located in the Thermal and Aeraulic Machines laboratory at the University of Padova is sketched in Fig.2. The figure reports the instrumentation accuracy, as well.

The following two paragraphs focus on the features of the experimental setup that are most important for this work.

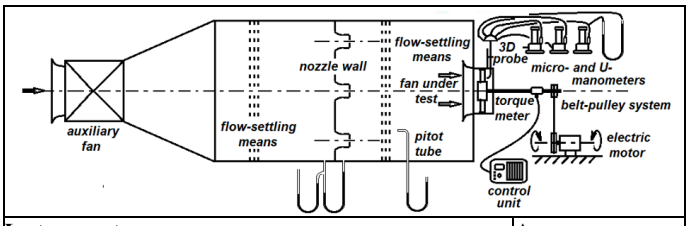

Instruments	**Accuracy**
Water micro-manometers	±0.05mm H_2O
Water U-manometer	± 0.2 mm H_2O
Rpm counter	± 2 rpm
AEP μTOR torque meter (linearity and hysteresis)	± 0.01 N x m
Digital barometer	± 100 Pa
Wet-and dry bulb thermo-resistors	± 0.1 K
Test chamber thermo-resistor	± 0.1 K

FIGURE 2: SCHEME OF THE UPGRADED LAYOUT OF THE FAN TEST RIG AT THE AERAULIC AND THERMAL MACHINES LAB OF THE UNIVERSITY OF PADOVA.

2.1.1 Fan test rig

The details of the test rig in its original layout were described in previous publications by the authors (see e.g. [21]). It is a Type-A installation, compliant with the ISO-5801 standard [19]. Some modifications were made to improve the accuracy and the ease of use of this rig.

The thermometers required to determine the ambient condition and air mass density ρ, namely the wet and dry bulb temperatures and air temperature in the test rig chamber (affecting the fan volume flow rate q_v) have been substituted by three pt100 thermo-resistors connected to the Arduino Uno Rev3 board. The temperature sensors have been calibrated using the output recorded by each of them at 0°C and 100°C (they were immersed in a mix of cold water and ice, and in boiling water, respectively). This experimental setup permits quantifying both the environment and air flow conditions at each experimental point. This detailed acquisition procedure reduces some unphysical undulations in the aerodynamic performance curves, but is not imposed by the standard, which admits average values. In addition, the original torque crane has been substituted by a torque meter AEP (mod. μTOR) mounted between the rotor shaft and the shaft at the exit of the belt-pulley system that is used to multiply the rotational speed of the electric motor (driven by an inverter). The voltage output of the torque meter is converted into Nxm torque data by an HBM® amplifier system (mod. MGC). The torque data, and consequently the efficiency data, matched almost perfectly the data measured with the original torque crane. A direct comparison of the same data set measured with the different experimental setups is not shown here. Figure 3 presents data already published in [20], enriched with the performance curves at ϕ_P = 22°, measured with the new experimental setup. The validation of this setup is indirectly assessed by the continuous and strictly concave envelope of the efficiency curves.

The uncertainty in the measurements of the aerodynamic global performance parameters is certainly reduced compared to that estimated using the previous experimental setup [20]. Accordingly, uncertainties lower than 1.26%, 0.94% and 1.97% are expected at best efficiency duty for the mass flow rate, fan pressure and aeraulic efficiency parameters, respectively.

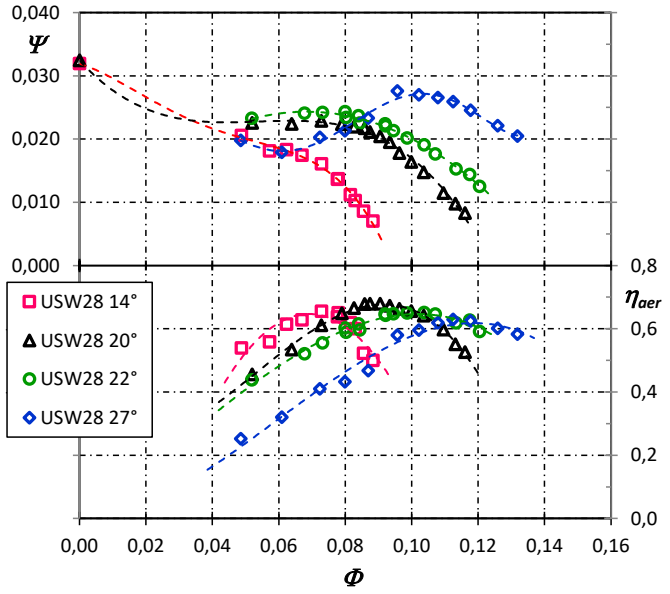

FIGURE 3: PRESSURE COEFFICIENT (UPPER) AND AERAULIC EFFICIENCY (LOWER) VS FLOW RATE COEFFICIENT FOR THE USW28 FAN MEASURED AT SEVERAL BLADE POSITIONING ANGLES.

2.1.2 Local velocity measurements

The radial distribution of the pitch averaged air velocity in a section just downstream of the rotor exit has been measured using the five-hole 3D directional probe DA-187-12-F-10-CD by United Sensors Corp.®. The support of the probe has been mounted on the USW28 fan casing, which has been drilled to immerse the probe in the air flow at 29.8mm behind the blade stacking line (see, Fig. 4). Accordingly, the measurement plane *2'* is placed approximately 14mm downstream of the blade trailing edge at the hub. The positioning of the probe so close to the rotor exit hinders very high-quality pitch-averaged velocity measurements because of the rather strong periodic fluctuations caused by the blade passage and the not yet fully satisfied radial equilibrium condition. However, this is the easiest solution to keep the other characteristics of the free-outlet type-A installation unchanged.

The differential pressure measurements required to quantify the local velocity magnitude and the radial velocity component are performed with two water micromanometers. An inclined tube manometer permits to check the zeroing of the differential pressure between the two holes occurring when the probe is positioned at the right value of the yaw angle $\alpha_{2'}$.

The estimated uncertainty on the yaw angle is approximately equal to ±1°. The yaw angle affects the indirect measurements of the axial and tangential velocity components: the uncertainty on these data is not lower than ±0.5% and ±3%, respectively.

The reliability of the local velocity measurements has been checked by evaluating the spanwise distribution for Φ = 0.099, Ψ = 0.020, at ϕ_P = 22°. Their dimensionless values i.e., the axial velocity ratio Σa, the swirl coefficient εs, and absolute flow exit

angle $\alpha_{2'}$ are shown in Fig. 5 with circle, triangle, and diamond markers, respectively.

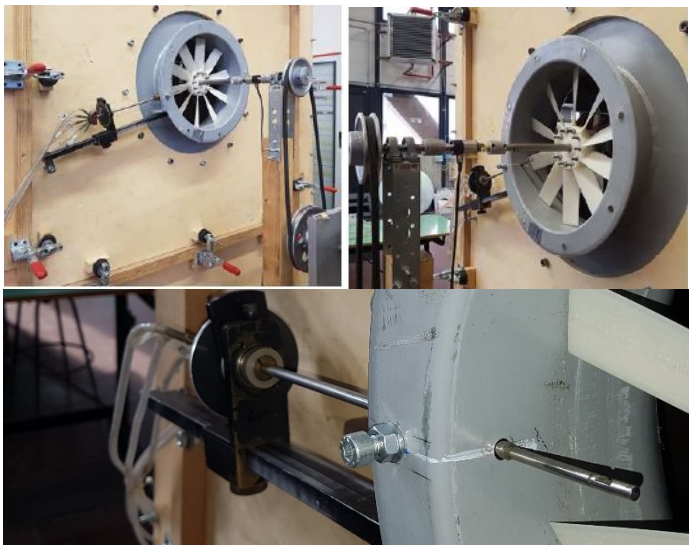

FIGURE 4: EXPERIMENTAL SETUP USED FOR THE LOCAL VELOCITY MEASUREMENTS –3D PROBE POSITIONING SYSTEM (UPPER LEFT FRAME); LOCATION OF THE MEASUREMENTS STATION (UPPER RIGHT FRAME); DETAILED VIEW OF THE 3D PROBE INSTALLATION (LOWER FRAME).

To permit a preliminary validation, Fig.5 also shows the dashed lines with empty markers indicating the corresponding theoretical design values at Φ_D = 0.097 and ϕ_P = 20°. The experimental distribution of $\alpha_{2'}$ is in good agreement with the design distribution of the yaw angle α_2 downstream of the rotor.

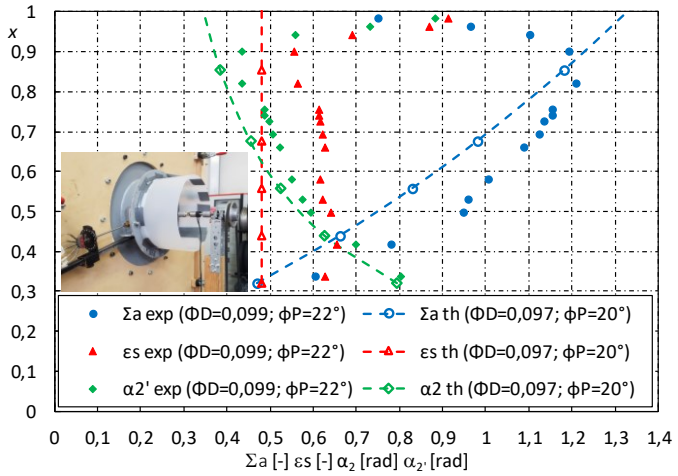

FIGURE 5: DESIGN (TH) AND EXPERIMENTAL (EXP) SPANWISE DISTRIBUTIONS OF THE AXIAL VELOCITY RATIO, SWIRL COEFFICIENT, AND ABSOLUTE FLOW EXIT ANGLE AT THE ROTOR DOWNSTREAM.

On the other hand, a measured obliquity of Σa lower than the design one is consistent with the experimental value of Φ, which is higher than Φ_D. The higher measured values of εs confirm the higher value of ϕ_P settled in the experiments. Note that, this set of experimental measurements was performed on a modified configuration of the USW28 fan, in which the casing was slightly elongated in the region downstream of the rotor, while the position of the measurements plane was kept unchanged (see the picture embedded on the left-hand side of Fig. 5). This modification was made to permit an even comparison. In fact, an elongated casing should limit the radial diffusion at the rotor exit, which is expected in a test rig belonging to the Type-A installation category.

2.2 Computational Fluid Dynamics

A previous work of the authors [22] demonstrated that steady-state single-channel calculations performed on a simplified meridional geometry defined by a straight annular portion (disregarding electric motor, bell-mouth entry and struts) permit a good fit of the global aerodynamic performance data in the fan operation range around the best efficiency duty point. It was concluded that such modelling approach is best suited to support the designer work after the preliminary sizing of the fan. Accordingly, it has been chosen here to perform several steady-state calculations of the USW28 fan on a domain defined by a single-blade channel including the blade tip clearance. The goal is to predict values of the aerodynamic performance not dependent on the grid density. The sensitivity of the results on different turbulence models has been investigated as well. The results of these calculations and the descriptions of the main features of the CFD models are reported in the following three sub-sections. The first and the third sub-sections focus on simulations of different accuracy levels performed with two state-of-the-art commercial CFD packages, namely: Star CCM+ ver.14.02.010-R8 and open-source OpenFOAM v1812 library. These simulations have been used as numerical benchmarks for the CFD approach based on MULTALL 18.3, described in the second sub-section.

2.2.1 CFD Benchmark: Star CCM+ model

The study considers three different lengths of the channel branches before and after the rotor and three different turbulence closures namely, the high-Reynolds standard K-ε [23], the two-layer non-linear K-ε Realizable [24], and the low-Reynolds K-ε model suggested by Lien [25].

An O-type structured grid has been used to mesh the domain surrounding the rotor, whereas two structured blocks obtained by axial extrusion of the two cylindrical crown sectors defining the inlet and exit surfaces of the rotor sub-domain, have been used to discretise the upstream and downstream channel pieces that define the annulus. All the computational domains, independently of their axial extension, feature a near wall grid refinement with grid clustering dependent on the grid density (3 meshes have been considered). The wall y^+ value depends on the

selected turbulence model. The main features of the simulations set are summarised in Tab.3.

TABLE 3: CFD SETUP OF THE 27 MODELS USED IN THE SIMULATIONS PERFORMED WITH STAR CCM+

RANS - turbulence closure			
K-ε model version	Standard high-Re [23]	Low-Re by Lien [24]	Non-linear realizable [25]
Near-wall treatment	Standard wall function	all y^+ wall treatment	Two layer ‡ + all y^+ wall treatment
Wall y+	>25	~1	~1
Domain size (approx. mm/chordlengths)			
	Short	**Medium**	**Long**
Rotor upstream	20mm / 0.7	40mm / 1.3	50mm / 1.5
Rotor	60mm/2	60mm/2	60mm/2
Rotor downstream	50mm / 1.5	115mm / 3	190mm / 5
Grid density (grid points)			
	Coarse	**Medium**	**Refined**
Rotor	80 x 20 **	140 x 38 **	260-280 x 74 **
tip gap	6	6	12
Rotor upstream	20 x16 x 5-8 §	38 x 32 x 8-10 §	74 x 64 x 10-14 §
Rotor downstream	20 x 16 x 8-18 §	38 x 32 x 14-30 §	74 x 64 x 20-34 §
Total	~50k	~300k	~1400k
			** *O-path x spanwise*
			§ *span x pitch x streamwise*

Uniform total pressure and fixed mass flow were used as boundary conditions at the inlet and outlet of the domain, respectively. A residual in the order of 10^{-5} was the maximum value allowed. Most of the performed computations reached residuals lower than this limit by an order of magnitude in all the transport equations solved with the segregated pressure-based approach [26]. Figure 6 shows some details of the medium domain size and medium density computational grid.

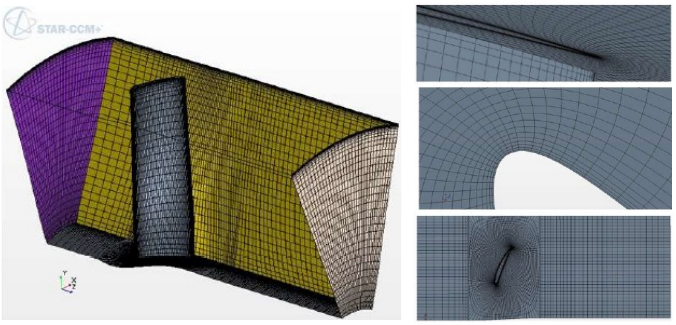

FIGURE 6: ENTIRE DOMAIN (LEFT), TIP CLEARANCE DETAIL (UPPER RIGHT), TRAILING EDGE CLUSTERING (MIDDLE RIGHT), CASING SURFACE (LOWER RIGHT) OF THE MEDIUM DOMAIN SIZE AND MEDIUM GRID DENSITY.

The main outcomes of the study performed to numerically validate the CCM+ models are:

a) The lengthwise extension of the domain plays a very minor role in the predictions of the global aerodynamic performance. For example: at $\phi_P = 22°$ and $\Phi = 0.0895$, the calculations performed on the refined grid with the *K-ε* realizable turbulence closure predict values of the (Ψ, η_{aer}) pair that ranges from (0.024, 0.69) to (0.0235, 0.68) moving from the short to the long size domain. A slightly more pronounced difference was found in the velocity profiles downstream of the rotor.

b) Noticeable differences exist between the results predicted by calculations performed using different turbulence models, as shown in Fig.7.

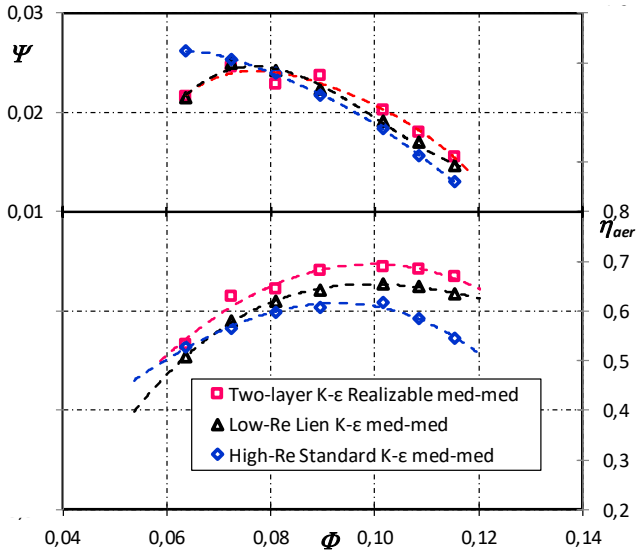

FIGURE 7: SENSITIVITY OF THE GLOBAL AERODYNAMIC PERFORMANCE ON THE TURBULENCE MODEL (FOR THE MEDIUM DOMAIN SIZE AND MEDIUM GRID DENSITY).

c) The minimum cell numbers required to obtain predictions that no longer depend on the grid density is affected by the turbulence model used in the computations. The calculations with the low-Reynolds model depend strongly on grid density. Figure 8 shows the dependence of the results on the grid density (compare the curves obtained using the same turbulence model) and how the turbulence model affects such dependence (compare the upper and lower frames in Fig. 8).

Note that the Two-layer non-linear *K-ε* calculations performed on the medium density grid predicted an oscillating behaviour of both the pressure coefficient and the aeraulic efficiency datum at the duty point close to the maximum pressure flow rate in the unstable fan operation range. Accordingly, both the minimum and maximum values of the pressure coefficient predicted at this operation have been reported in Fig.8 because they feature equal value of the residuals.

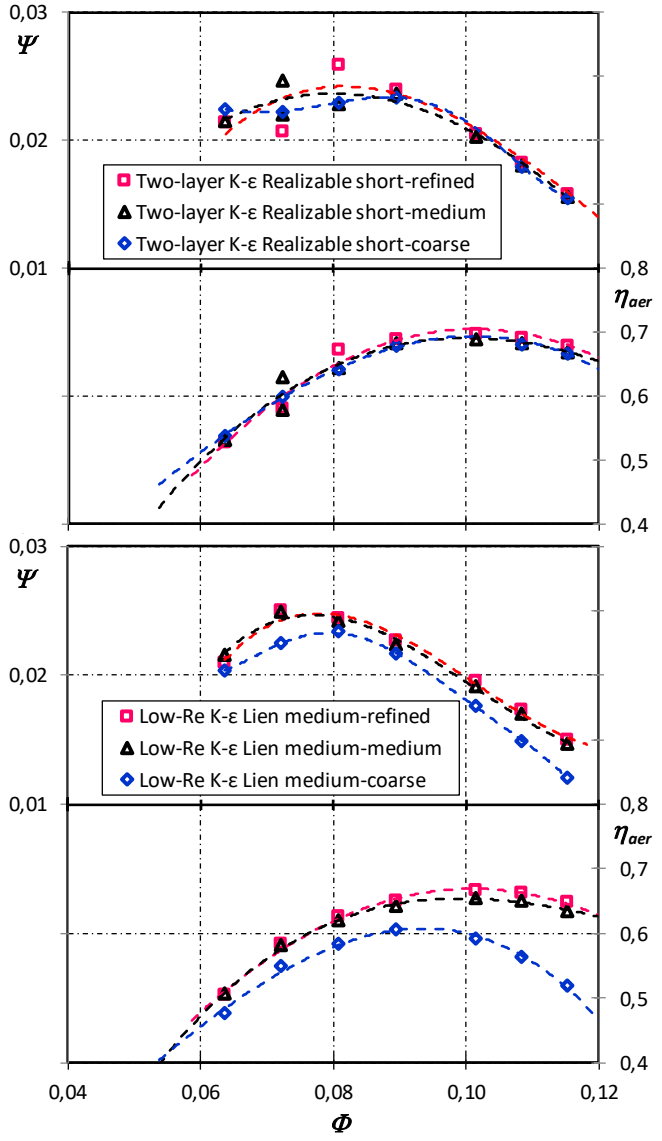

FIGURE 8: SENSITIVITY OF THE GLOBAL AERODYNAMIC PERFORMANCE ON THE GRID DENSITY FOR DIFFERENT TURBULENCE MODELS (TWO-LAYER K-E REALIZABLE MODEL – UPPER, K-E LOW RE LIEN MODEL - LOWER) AT FIXED DOMAIN SIZE.

Figure 8 (lower) also shows that the results of the more refined grid calculations could still depend on the grid density. The average changes of the pressure coefficient and efficiency values are approximately -1.3% and -1.2% when the grid coarsens from the refined to the medium density one, and approximately -2% and -1.5% when the grid coarsens even further from the medium density to the coarser one. These outcomes suggest that grid independent calculations (i.e., calculations on grids counting more than 1M cells) are not compatible with the computational effort commonly accepted by fan manufacturers for preliminary design computations. Accordingly, a proper set of grid density and turbulence model should be chosen to achieve an acceptable trade-off between quality of the CFD predictions and their computational cost.

2.2.2 CFD approach based on MULTALL

A study similar to the one reported in sub-Section 2.2.1 has been performed on the steady-state flow models implemented in MULTALL ver.18.3. The study considers two different lengths of the channel branches before and after the rotor, and two different turbulence closures namely the zero-equation mixing length [27] and the one-equation Spalart-Allmaras [28] models in their high-Reynolds version implemented in MULTALL (i.e., with the standard wall function treatment). The mixing length model calculations showed higher stability and convergence rate. Moreover, this model demonstrated remarkable tolerance to the highly skewed grid used by MULTALL in the blade tip region to account for the tip clearance flow. Accordingly, the mixing length model, which is the MULTALL default option, has been selected.

The computational domains have been meshed with a fully structured grid with a near wall refinement and a grid clustering, both depending on the grid density. The wall y^+ value varies from 0.05 to 10. Note that the limiting y^+ value implemented in the code to switch on the standard wall function approach is equal to 5. Thus, the code solves the boundary layer in some regions while switches to the standard wall function treatment in others.

Table 4 summarises the main features of the simulations performed with MULTALL.

Uniform inlet total pressure and outlet static pressure were considered as boundary conditions. The calculations were performed in the fully-incompressible mode implemented in MULTALL to solve the steady-state RANS equations with the density-based algorithm [15].

TABLE 4: CFD SETUP OF THE 12 MODELS USED IN THE SIMULATIONS PERFORMED WITH MULTALL

RANS - turbulence closure		
Model	Mixing length [27]	Spalart-Almaras [28]
Near-wall treatment	Standard wall function/all y^+ wall treatment	
Wall y^+	>5/<5	
Domain size (approx. mm/chordlengths)		
	Short	**Medium**
upstream	30mm/1	75mm/2.5
Rotor	30mm/1	30mm/1
downstream	60mm/2	125mm/4.2

Grid density (grid points)			
	Coarse	**Medium**	**Refined**
upstream	24 x 24 x 24 §	46 x 46 x 44 §	64 x 64 x 64 §
Rotor	24 x 24 x 24 §	46 x 46 x 64 §	64 x 64 x 90 §
tip gap	5	10	15
downstream	24 x 24 x 48 §	46 x 46 x 76 §	64 x 64 x 150 §
Total	~55k	~390k	~1250k

§ *span x pitch x streamwise*

Finally, the MULTALL-CFD approach splits each calculation into two steps. The first step serves as initialisation, to approach a rough estimation of the flow field: it counts 15000

iterations performed with the Courant-Friedrichs-Lewy (CFL) solver parameter [26] set to 0.1. The second is a refinement step: it counts 7500 iterations with the CFL parameter set to 0.04. The higher value of CFL used in the first step allows for faster convergence rate but higher instability, which impedes obtaining a satisfactory degree of convergence. In contrast, the lower CFL used in the second step allows each computation to reach values of the average residual (defined as the average percentage change in velocity per time step divided by the RMS velocity of all grid points) and continuity error lower than 0.0012 and 0.01, respectively.

Figure 9 shows some details of the medium-size medium-length computational grid.

As per the results of the CCM+ models, MULTALL calculations confirmed that the streamwise length of the domain does not alter the aerodynamic performance when the domain extends by more than 2.5 and 4.2 chordlengths, upstream and downstream of the rotor, respectively.

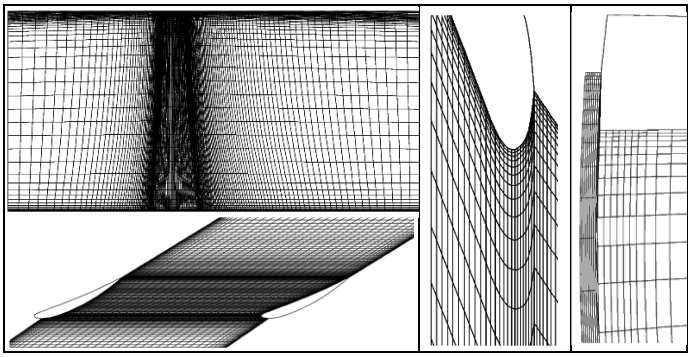

FIGURE 9: MERIDIONAL SECTION (UPPER LEFT), STREAM SURFACE PROJECTION (LOWER LEFT), LEADING EDGE CLUSTERING (MIDDLE), AND TIP CLEARANCE DETAIL (RIGHT) OF THE MEDIUM DOMAIN SIZE AND MEDIUM DENSITY GRID.

In summary, to conclude about the numerical validation of MULTALL models:

a) Grids having cell numbers approximately higher than 400k allow predictions of the global aerodynamic performance that do not depend on the grid density, for a given turbulence model. The insensitivity to the turbulence model was largely expected in view of the basic turbulence modelling implemented in MULTALL and the many near wall regions solved with the standard wall function treatment.

b) The trends of both the fan pressure and aeraulic efficiency curves are satisfactorily predicted in the entire stable operation range of the fan, irrespective of the turbulence model or grid density.

2.2.3 Detailed CFD Benchmark: OpenFOAM model

As per the previous models, the flow was assumed to be incompressible and the steady-state RANS approach was used. Turbulence closure relied on the cubic low-Reynolds formulation of the *K-ε* model [25]. The linearized system of equations was solved using the Generalized Algebraic Multi-Grid (GAMG) solver with a 10^{-6} convergence tolerance for pressure and smoothSolver with 10^{-8} convergence tolerance for all the other quantities. Convective terms in the equations were discretised using QUICK scheme, divergence terms with upwind scheme and Laplacian terms with central differences. Convergence of the simulations was checked against residuals of the simulation and characteristics of the fan (total-to-static pressure rise and torque on the blade). In contrast to the previous CFD benchmark, a high-fidelity calculation approach was chosen here to have detailed predictions of the local flow features at ϕ_P = 22°. Accordingly, the final model features a computational grid having 2.89M cells with hexahedra along the solid walls. Details of the CFD setup i.e., turbulence model features, domain size, mesh quality indicators and boundary conditions are given in Tab. 5, while an overview of the grid is shown in Fig. 10.

TABLE 5: CFD SETUP USED IN THE SIMULATIONS PERFORMED WITH OPENFOAM

RANS - turbulence closure			
Model	Cubic low-Reynolds K-ε [25]		
Near-wall treatment	Standard wall functions		
Wall y^+	**Min**	**Max**	**Average**
Blade	3.3	186.4	53.6
Hub	4.0	113.6	37.0
Casing	1.3	242.8	77.5
Domain size (approx. mm/chordlengths)			
upstream	80mm/2		
Rotor	40mm/1		
downstream	80mm/2		
Mesh quality indicators (2.89M cells)			
	Min	**Max**	**Average**
Volume ratio	1	131	2.32
Aspect ratio	0.32	33.1	4.84
Min. included angle	10.3	90	56.2
Centroid skewness	0	0.75	0.11
Boundary conditions			
Inlet	volume flow rate		TI=5%, l= 0.016 m
Outlet	Zero gradient		
Pitchwise surfaces	periodicity		

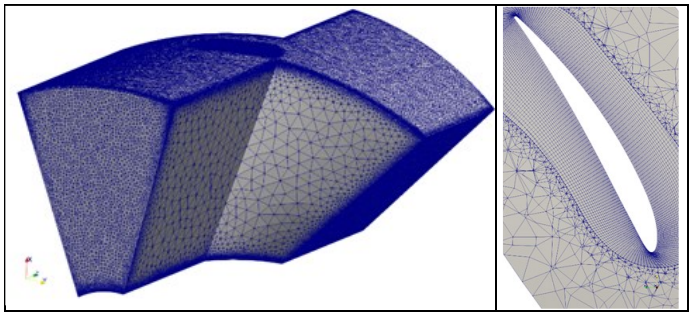

FIGURE 10: OPENFOAM MODEL GRID - PERSPECTIVE VIEW OF THE ENTIRE DOMAIN GRID (LEFT); DETAIL OF THE GRID SURROUNDING THE BLADE SURFACE (RIGHT).

3 Results

This section presents in its first sub-section the numerical validation of the CFD approach based on MULTALL previously presented. The second sub-section focuses on the comparison between the CFD predicted and EFD measured data. Note that many of the corresponding operation points simulated with different CFD codes and compared in the following sub-sections feature slightly different values of the flow rate coefficient. This is because different sets of boundary conditions were required to reach a satisfactory level of convergence depending on the code.

3.1 Comparison between CFD results

Figure 11 compares the aerodynamic performance curves predicted by MULTALL with the corresponding curves predicted by the CCM+ simulations of the medium domain size and medium grid density shown in Fig.8, and with the OpenFOAM simulations described in sub-Section 2.2.3.

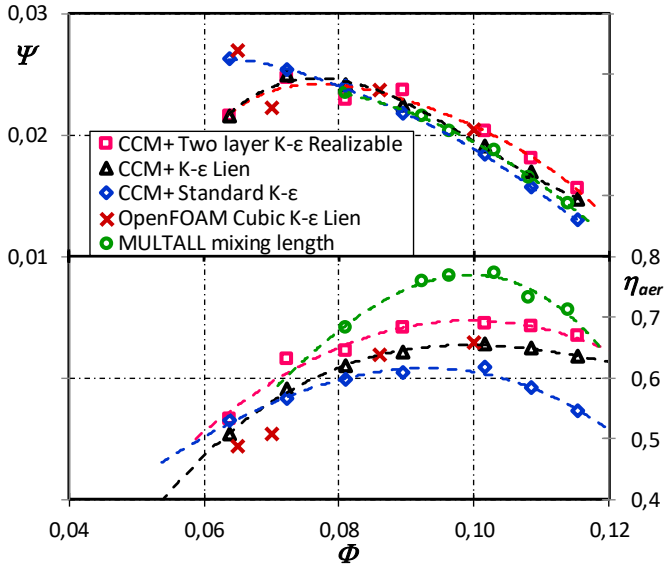

FIGURE 11: DIMENSIONLESS AERODYNAMIC PERFORMANCE CURVES OF THE USW28 FAN PREDICTED BY MULTALL, OPENFOAM AND CCM+ (WITH DIFFERENT TURBULENCE CLOSURES) FOR THE MEDIUM DOMAIN SIZE AND MEDIUM GRID DENSITY.

Figure 11 clearly indicates that the pressure curve of the USW28 fan predicted by MULTALL is in very good agreement with the CCM+ predictions obtained with the K-ε Lien turbulence model, whereas it underestimates by a noticeable amount the Ψ curve predicted by the two-layer non-linear K-ε realizable CCM+ model and data obtained by the detailed OpenFOAM simulations with the Lien's cubic K-ε model. On the other hand, η_{aer} of the USW28 fan predicted by MULTALL overestimates all the other corresponding predictions especially in the surrounding of the maximum efficiency duty. The overestimation increases when passing from the K-ε realizable predictions to the K-ε Lien to the standard K-ε, in that order. The detailed CFD simulations with OpenFoam predict η_{aer} values almost equal to those predicted by CCM+ with the low-Re K-ε model by Lien in the stable operation range of the fan. However, all the CFD simulations of the USW28 aeraulic efficiency predict that maximum η_{aer} occurs at the same value of the flow rate coefficient. This leads to conclude that MULTALL predicts the trends of aerodynamic performance curves and the best efficiency duty point with the same reliability level as state-of-the-art RANS CFD codes.

Figure 12 shows the spanwise distribution of Σa, εs and Σr at the measurement plane *2'* as predicted by the simulations of the $\Phi \approx 0.10$ duty, performed with MULTALL, CCM+ and OpenFOAM. To allow for a clear comparison, Fig.12 reports only the CCM+ results obtained with the Lien's model.

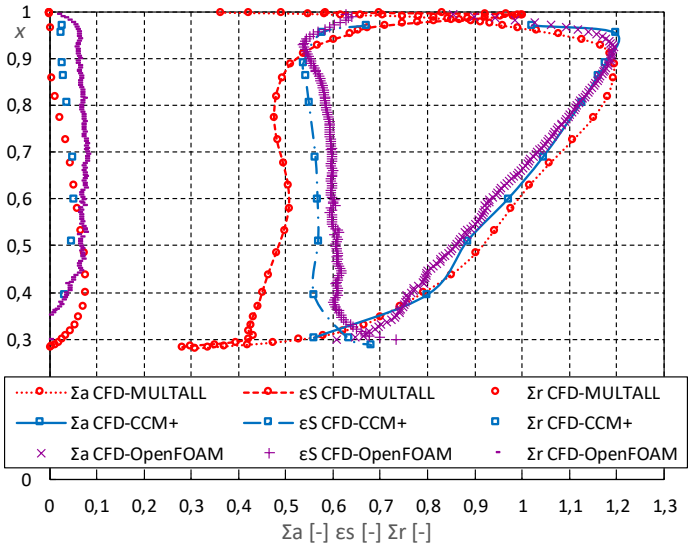

FIGURE 12: DIMENSIONLESS VELOCITY COMPONENTS PREDICTED AT THE MEASUREMENT PLANE 2' BY MULTALL CCM+ AND OPENFOAM AT $\Phi \approx 0.1$ AND 22° BLADE POSITIONING ANGLE (MEDIUM DOMAIN SIZE AND MEDIUM GRID DENSITY).

As a general comment, both the trends and values of all the velocity components are in very good agreement. In particular, the three sets of axial velocities (i.e., the three data curves having highest abscissae in Fig.12) almost overlap in the lower fraction of the blade span, whereas they slightly differ in the outer fraction of the blade channel, where MULTALL predicts a smoother decrease towards the casing wall. This different behaviour is compatible with a different estimate of the contribution of the tip leakage flow on the mean axial velocity profile. The different behaviour of the axial velocity reflects the different decrease of the tangential velocity ratio εs predicted by the three codes (see the three curves in the middle of the diagram).

It is worth noting the lower average value of εs predicted by MULTALL in comparison to both CCM+ and OpenFOAM. A different estimate of the straightening effect of the pipe at the rotor exit reasonably plays a role on the amount of residual swirl at the measurement plane.

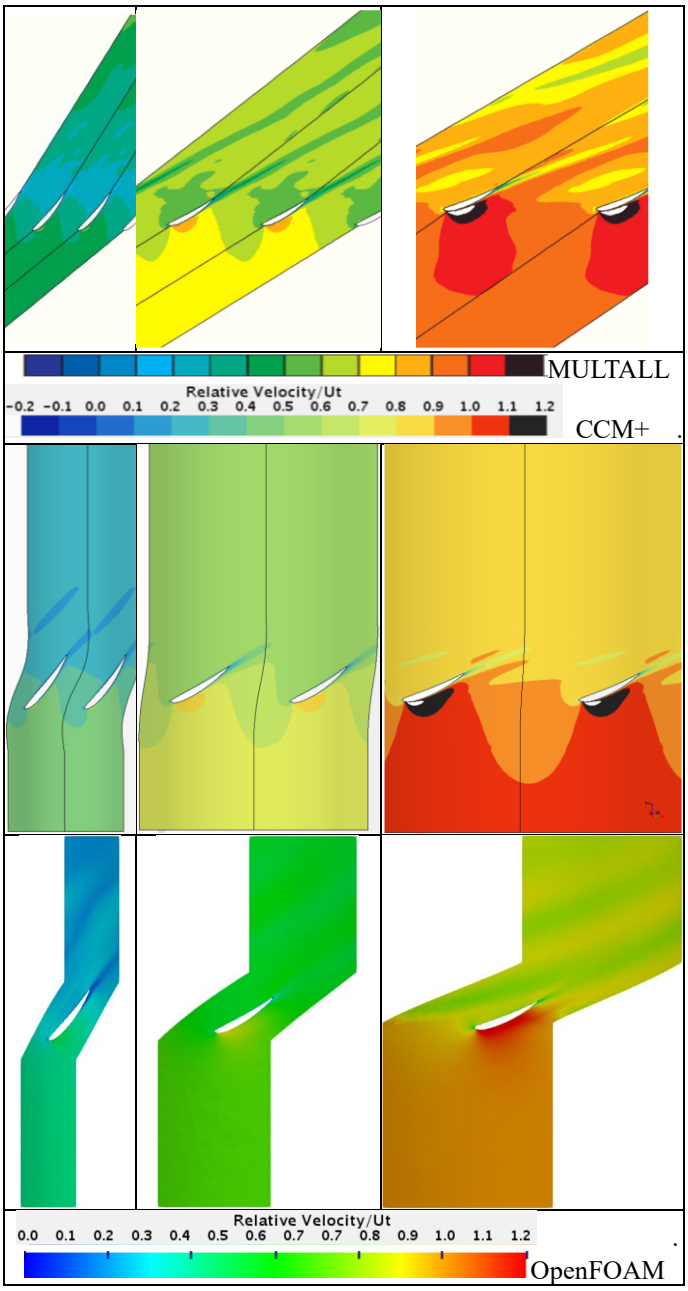

FIGURE 13: RELATIVE VELOCITY CONTOURS AT 5% (LEFT), 50% (CENTRE), 95% (RIGHT) OF BLADE SPAN AS PREDICTED BY MULTALL AND CCM+ (AT $\Phi = 0.102$) AND OPENFOAM (AT $\Phi = 0.086$). THE BLADE POSITIONING ANGLE IS EQUAL TO 22°.

Figure 13 compares the contour plot of the relative to tip velocity ratio computed by MULTALL, CCM+ and OpenFOAM at operations close to the maximum aeraulic efficiency duty. The figure allows a deeper insight on the differences in the features of the local flow field as predicted by the three CFD codes on three cylindrical sections located at 5%, 50% and 95% of the blade span. It is worth noting that MULTALL predicts a less uniform velocity field than both the state-of-the-art codes, as if it were able to capture details of the flow field that are not resolved by either CCM+ or OpenFOAM. However, the support of experimental measurements, not yet available, is mandatory to confirm this result.

Finally, the computation time estimated to simulate the best efficiency operation on a single core of an 2GHz Intel Duo® processor is approximately: (i), 300mins - for MULTALL grid *independent* calculation (medium density grid); (ii), 65mins - for CCM+ grid *dependent* calculation (medium density grid); and (iii), 750mins - for the OpenFOAM detailed computation. Thus, if calculations at equal grid density are concerned, the use of MULTALL should not be recommend, since it requires a computation time noticeably higher if compared to state-of-the-art codes. On the other hand, if numerically validated calculations of the global-aerodynamic performance (i.e., grid-independent predictions) are concerned, the present findings stated that the computational effort required is approximately unaffected by the adopted CFD code. In fact, it is expected that CCM+ grid independent results require grid densities and computation times not much lower than those required by OpenFOAM calculations and, very likely, higher than those required by MULTALL. Moreover, the flexibility in the management of the blade geometry allowed by the MULTALL data input system is very interesting for fan designers: once the 2-D aerofoil coordinates have been uploaded, the analysis of fan designs implementing different three-dimensional stacking of the blade becomes straightforward [29].

3.2 Experimental validation of the CFD approach based on MULTALL

In Fig. 14, the global aerodynamic performance predicted by the CFD approach based on MULTALL are compared with the experimental data. Figure 14 also shows the CCM+ predictions obtained with the K-ε Lien turbulence model and the results of the detailed OpenFOAM computations.

The experimental pressure curve of the USW28 fan is predicted very well by MULTALL in the entire stable operation range. No appreciable differences exist between MULTALL, CCM+ and OpenFOAM predictions. In contrast, the aeraulic efficiency predicted by MULTALL overestimates by approximately 20% the experimental data and CCM+ and OpenFoam results, especially in the operation range around the best efficiency duty. Looking at fan operation towards free delivery, MULTALL overestimates the aeraulic efficiency by approximately 20% and 15% if compared to the experimental data and state-of-the-art CFD results, respectively. However, the best efficiency flow rate coefficient is very well captured.

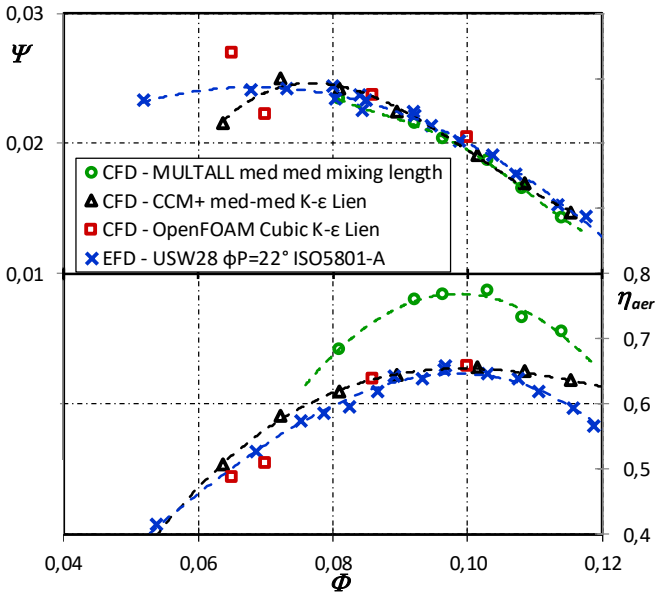

FIGURE 14: USW28 AERODYNAMIC PERFORMANCE PREDICTED BY MULTALL (CIRCLES), CCM+ (TRIANGLES) AND OPENFOAM (SQUARES), AND MEASURED ACCORDING TO ISO5801 (CROSSES) AT 22° BLADE POSITIONING ANGLE.

Figure 15 compares the CFD results and EFD spanwise distributions of the dimensionless velocity components (Fig.15 upper) and yaw and pitch angles (Fig. 15 lower) of the absolute flow measured by the 3D probe at the *2'* plane. Both predictions of the axial and tangential velocity components obtained by MULTALL, CCM+ and OpenFOAM are in satisfactory agreement with the experimental data. In particular, the spanwise distribution of εs is predicted better by the two state-of-the-art CFD codes, although the undulations of the curve are very well described by MULTALL. At mid-span, MULTALL underestimates the tangential velocity component by approximately 15% and 10% if compared to the experimental data and predictions of the other CFD codes, respectively. The experimental distribution of Σa appears to be captured slightly better by MULTALL, whereas all the CFD results strongly underestimate the radial velocity component measured by the 3D probe. However, it is worth considering that (i) the magnitude of Σr data could be affected by the radial diffusion occurring at the fan exit in a Type-A installation test and (ii) the accuracy of Σr data is rather limited because of the difficulty in measuring very low values of differential pressure.

Note that, MULTALL well predicts the slope of the yaw angle distribution and the behaviour of the pitch angle. The wide pitch angle measured in the outer part of the span could be partially affected by some leakage across the hole, which was drilled in the casing to allow the immersion of the probe, and may cause a local excess of radial motion.

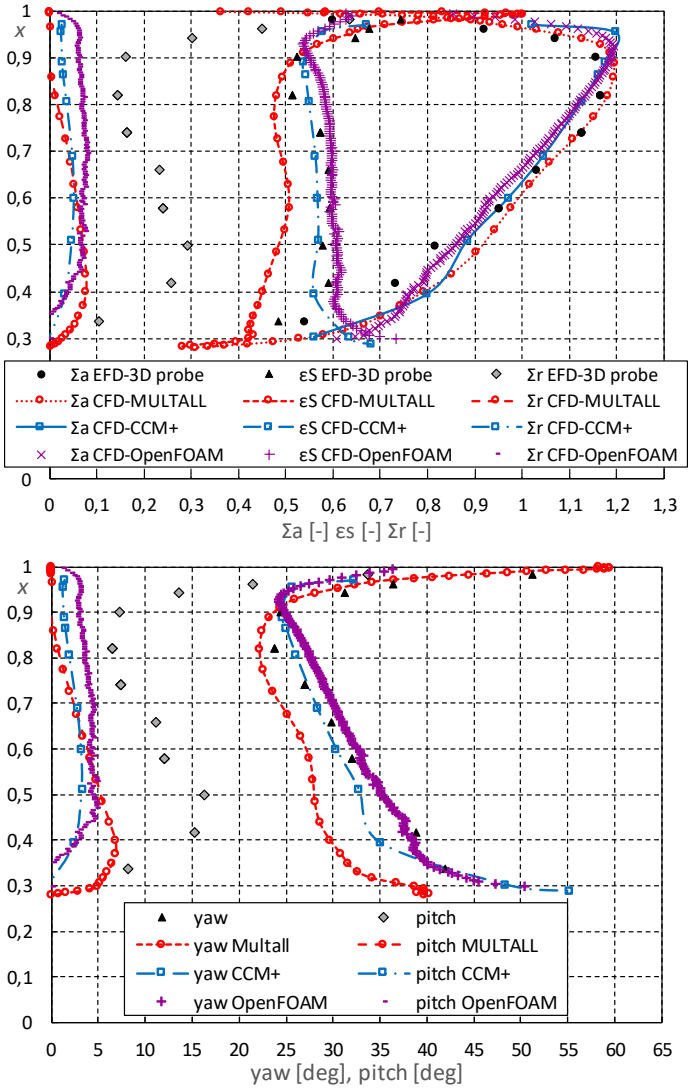

FIGURE 15: DIMENSIONLESS VELOCITY COMPONENTS (UPPER) AND PITCH AND YAW ANGLES (LOWER) PREDICTED BY MULTALL, CCM+ AND OPENFOAM, AND MEASURED BY THE 3D PROBE AT $\Phi \approx 0.1$ AND 22° BLADE POSITIONING ANGLE. ALL THE REPORTED DATA REFER TO PLANE 2' PLACED APPROXIMATELY 14MM DOWNSTREAM OF THE ROTOR.

CONCLUSIONS

A CFD approach for the analysis of axial-flow fans based on the open source code MULTALL has been presented and applied to a low hub-to-tip ratio tube-axial fan.

The trends of the global aerodynamic performance curves and the best efficiency duty point, as well as trends and values of all the local velocity components downstream of the rotor predicted by MULTALL resembled the corresponding predictions obtained by state-of-the-art RANS CFD codes.

The comparison of the MULTALL results with the experimental data showed that:

- In terms of global aerodynamic performance, MULTALL predicts well the pressure curve of the fan in the stable operation range, whereas it overestimates the aeraulic efficiency curve, especially in the operation range around the best efficiency duty. However, the best efficiency flow rate is captured very well.
- In terms of the local flow field, MULTALL predicts fairly well the axial and tangential velocity components, the slope of the yaw angle distribution, and the behaviour of the pitch angle downstream of the rotor.

This leads to the conclusion that MULTALL can be used as a CFD tool for the analysis of low-speed axial-flow fans, especially in the preliminary design phase where it is most important to verify whether the target flow rate and the corresponding pressure are fulfilled at best efficiency operation and where a rapid comparison of different blade designs helps selecting the more promising blade geometry. On the other hand, the noticeable overestimation of the efficiency requires further investigations. The present results suggest that the mixing length turbulence modelling implemented in MULTALL does not allow capturing all the loss mechanisms at the same detail level as state-of-the-art CFD codes. Accordingly, it is planned to try implementing in MULTALL a new wall function based on machine learning: the preliminary tests on the potentialities of such approach led to promising results in [30].

ACKNOWLEDGEMENTS

The authors acknowledge Gianfranco Zanon for his contribution in improving the mechanical quality of the experimental facility.

NOMENCLATURE

$AR = B/l$	blade aspect ratio, [-]
B	blade height, [m]
C_L, C_D	aerofoil lift and drag coefficients, [-]
CFD	computational fluid-dynamics
D	rotor diameter, [m]
EFD	experimental fluid-dynamics
P	mechanical power at fan rotor, [W]
R_a	surface roughness, [μm]
U	peripheral blade speed, [m/s]
Z	rotor blade number, [-]
c_a	mean axial velocity in the annulus, [m/s]
d	aerofoil nose droop, [m]
h	aerofoil maximum camber, [m]
i	incidence angle, [°]
l	aerofoil chord, [m]
p_f	fan pressure (ISO 5801), [Pa]
q_v	fan volumetric flow-rate, [m^3/s]
r	radial coordinate, [m]
t	aerofoil maximum thickness, [m]
tc	tip clearance, [m]
$x = 2r/D$	dimensionless radial coordinate, [-]

Greeks

α	yaw angle between axis and absolute flow, [°]
$\varepsilon s = c_{u2}/c_a$	local swirl coefficient at rotor outlet, [-]
θ	aerofoil camber angle, [°]
$\eta_{aer} = q_v\, p_f / P$	fan aeraulic efficiency, [-]
ν	hub-to-tip ratio, [-]
ρ	mass density, [kg/m^3]
$\sigma = l\, Z/(2\pi r)$	local blade solidity, [-]
$\phi_P = \pi/2 - \xi_t$	blade tip positioning angle, [°]
ξ	stagger (angle between chord and fan axis), [°]
ω	angular velocity, [rad/s]
$\Sigma a = c_{a2}/c_a$	local axial velocity ratio at rotor outlet, [-]
$\Sigma r = c_{r2}/c_a$	local radial velocity ratio at rotor outlet, [-]
$\Phi = q_v/\ \omega D^3$	fan flow rate coefficient, [-]
$\Psi = p_f\ /\ \rho\omega^2 D^2$	fan total pressure coefficient, [-]

Subscripts

$1, 2, 2'$	rotor inlet, exit, and downstream sections
D	design condition
a, r, t, th	axial, radial, tip and theoretical (design)

REFERENCES

[1] Bamberger, K., Carolus, T., 2015, "Design guidelines for low pressure axial fans based on CFD-trained meta-models", *11th European Conference on Turbomachinery Fluid Dynamics and Thermodynamics*, Madrid, Spain, March 23-27.

[2] Hirsch C., 1990, Numerical computation of internal and external flows, vol. II: Computational methods for inviscid and viscous flows, Wiley, New York.

[3] Denton, J.D., 1978, "Throughflow Calculations For Transonic Axial Flow Turbines", *J Eng Power Trans ASME,* Volume 100 (1978), Issue 2, Pages 212-218.

[4] Denton, J.D., July 1983, "An improved time-marching method for turbomachinery flow calculation", *Journal of Engineering for Gas Turbines and Power,* Volume 105, Issue 3, Pages 514-521.

[5] He, L., Denton, J.D., 1994, "Three-dimensional time-marching inviscid and viscous solutions for unsteady flows around vibrating blades", *Journal of Turbomachinery,* Volume 116, Issue 3, Pages 469-476.

[6] Denton, J.D., Xu, L., 1999, "The exploitation of three-dimensional flow in turbomachinery design", *Proceedings of the Institution of Mechanical Engineers, Part C: Journal of Mechanical Engineering,* Volume 213, Issue 2, Pages 125-137.

[7] Denton, J.D., 1992, "The calculation of three-dimensional viscous flow through multistage turbomachines", *Journal of Turbomachinery,* Volume 114, Issue 1, Pages 18-26.

[8] Denton, J.D., Dawes, W.N., 1999, "Computational fluid dynamics for turbomachinery design", *Proceedings of the Institution of Mechanical Engineers, Part C: Journal of Mechanical Engineering*. Volume 213, Issue 2, Pages 107-124.

[9] Pullan, G., Denton, J.D., and Dunkley, N., 2003, "An experimental and computational study of the formation of a

streamwise shed vortex in a turbine stage", *Journal of Turbomachinery*, Volume 125, Issue 2, Pages 291-297.
[10] Rosic, B., Denton, J.D.,and Pullan, G., 2006, "The importance of shroud leakage modeling in multistage turbine flow calculations", *Journal of Turbomachinery,* Volume 128, Issue 4, Pages 699-707.
[11] Kaschel, C.E., Denton, J.D., 2006, "Experimental and numerical investigation of the unsteady surface pressure in a three-stage model of an axial high pressure turbine", *Journal of Turbomachinery,* Volume 128, Issue 2, Pages 261-272.
[12] Crichton, D., 2007, "Fan Design and Operation for Ultra Low Noise", *PhD dissertation,* University of Cambridge, Engineering Department.
[13] Denton, J.D., 2010, "Some limitations of turbomachinery CFD", *Proceedings of the ASME Turbo Expo,* Volume 7, Issue PARTS A, B, and C, Pages 735-745.
[14] Persson, M., 2015, "Highly loaded HPT blading in KTH test turbine", *Thesis for the degree of Master of Science in Engineering,* Division of Thermal Power Engineering Department of Energy Sciences Lund University, Sweden.
[15] Denton, J.D., 2017, "Multall - an open source, computational fluid dynamics based, turbomachinery design system", *Journal of Turbomachinery,* Volume 139, Issue 12, Article number 121001.
[16] Tucker, P. G., 2013, "Trends in turbomachinery turbulence treatments", *Progress in Aerospace Science*, Volume 63: Pages 1-32.
[17] Cardillo, L., Corsini, A., Delibra, G., Rispoli, F., and Sheard, A.G., 2014, "A numerical investigation into the aerodynamic effect of pressure pulses on a tunnel ventilation fan", *Proceedings of the Institution of Mechanical Engineers, Part A: Journal of Power and Energy,* Volume 228, Issue 3, Pages 285-299.
[18] Angelini, G., Bonanni, T., Corsini, A., Delibra, G., Tieghi, L., and Volponi, D., 2017, "Optimization of an axial fan for air cooled condensers", *Energy Procedia*, Volume 126, Pages 754-761.
[19] ISO – International Organization for Standard - Technical Committee ISO/TC 117, Fans, "Industrial fans - Performance testing using standardized airways", ISO 5801:2007, CP 401 - 1214 Vernier, Geneva, Switzerland, 2007.
[20] Masi, M., Lazzaretto, A., 2019, "A New Practical Approach to the Design of Industrial Axial Fans: Tube-Axial Fans With Very Low Hub-to-Tip Ratio", *J. Eng. Gas Turbines Power*, Volume 141: pp. 101003-1/10.
[21] Castegnaro, S., Masi, M., and Lazzaretto, A., 2018, "Design and testing of an ISO 5801 inlet chamber test rig and related issues with the Standard", *Proceedings of FAN 2018 Conference,* Darmstadt, Germany, April 18-20.
[22] Masi, M., Lazzaretto, A., 2012, "CFD Models for the Analysis of Rotor-Only Industrial Axial-Flow Fans" *Proceedings of FAN 2012 Conference*, Senlis, France, April 18-20.
[23] Launder, B.E. Spalding, D.B., 1974, "The Numerical Computation of Turbulent Flows", *Computer Methods in Applied Mechanics and Engineering,* Volume 3, Pages 269-289.
[24] Shih, T.-H., Liou, W.W., Shabbir, A., Yang, Z. and Zhu, J., 1994, "A New k-e Eddy Viscosity Model for High Reynolds Number Turbulent Flows - Model Development and Validation", *NASA TM,* 106721.
[25] Lien, F.S., Chen, W.L., and Leschziner, M.A., 1996, "Low-Reynolds number eddy-viscosity modelling based on non-linear stress-strain/vorticity relations", *Proc. 3rd Symp on Engineering Turbulence Modelling and Measurements,* Crete, Greece, May 27-29.
[26] Versteeg, H. K., Malalasekera, W., 1995, An Introduction to Computational Fluid Dynamics: The Finite Volume Method, Longman Scientific and Technical.
[27] Prandtl, L., 1926, "Ueber Die Ausgebildete Turbulenz". *Proceedings 2nd International Congress Applied Mechanics*, Zurich, Switzerland, September 12-17.
[28] Spalart, P. R., Allmaras, S. R., 1992, "A One-Equation Turbulence Model for Aerodynamic Flows", *AIAA,* Paper 92-0439.
[29] Havakechian, S. Denton, J.D., 2015, "3D blade stacking strategies and understanding of flow physics in low pressure steam turbines. Part I – 3D stacking mechanisms", Proceeding of the ASME TurboExpo 2015. GT2015-42591. Montréal, Canada, June 15-19.
[30] Tieghi, L., Corsini, A., Delibra, G., Angelini, G., 2019, "Assessment of a Machine-Learnt Adaptive Wall-Function in a Compressor Cascade With Sinusoidal Leading Edge", Proceeding of the ASME TurboExpo 2019. GT2019-91238. Phoenix-AZ, US, June 17-21.